

PACS 71.15.Mb, 71.20.-b, 74.20.Pq

Electronic structure of Ag_8GeS_6

D.I. Bletskan, I.P. Studenyak, V.V. Vakulchak, A.V. Lukach

Uzhhorod National University

54, Voloshin str., 88000 Uzhhorod, Ukraine

E-mail: crystal_lab457@yahoo.com

Abstract. For the first time, the energy band structure, total and partial densities of states of Ag_8GeS_6 crystal were calculated using the *ab initio* density functional method in LDA and LDA+*U* approximations. Argyrodite is direct-gap semiconductor with the calculated band gap width $E_{gd} = 1.46$ eV in the LDA+*U* approximation. The valence band of argyrodite contains four energy separated groups of occupied subzones. The unique feature of electron-energy structure of Ag_8GeS_6 crystal is the energy overlapping between the occupied *d*-states of Ag atoms and the delocalized valence *p*-states of S atoms in relatively close proximity to the valence band top.

Keywords: argyrodite, electronic structure, density of states, density functional theory, spatial distribution of valence charge, chemical bond.

Manuscript received 21.10.16; revised version received 26.01.17; accepted for publication 01.03.17; published online 05.04.17.

1. Introduction

Germanium dichalcogenides are base materials for the synthesis of a wide class of superionic compounds known in $\text{M}_2\text{X}-\text{GeX}_2$ ($\text{M} = \text{Li}, \text{Na}, \text{Cu}, \text{Ag}; \text{X} = \text{S}, \text{Se}$) systems [1–3]. The ternary compound argyrodite (Ag_8GeS_6) with the mixed ionic-electronic conductivity type at room temperature, which transforms to the superionic state at the phase transition into the high temperature cubic modification, attracts the heightened interest among these compounds. The conductivity of synthesized Ag_8GeS_6 crystal is $\sim 10^{-3} \text{ Ohm}^{-1}\cdot\text{cm}^{-1}$ at $T = 293 \text{ K}$ [4].

From the practical viewpoint, the heightened interest in argyrodite is caused by the possibility to obtain it in the nanocrystalline state for use as a major construction component of the dye-sensitized solar cells (DSSCs) [5]. The further prospects of practical application of this compound are determined by the depth of understanding of formation nature of the

physical and chemical properties as well as finding the opportunities for their purposeful modification.

At this point, the physical properties of argyrodite are poorly studied. In literature, there are only data on the study of fundamental absorption edge [6, 7], photoconductivity [8] and electrical conductivity [4] of Ag_8GeS_6 crystals.

It is also very important to study electronic structure and chemical bonds in this silver-containing compound. The crystal structure complexity of this orthorhombic phase, the low lattice symmetry and the large number of atoms (60) in the unit cell make calculation of Ag_8GeS_6 electronic structure difficult.

This paper presents calculations of the energy band structure, total and local partial densities of states as well as spatial distribution of electronic charge density of Ag_8GeS_6 crystal performed using the density functional theory method in the local density approximation (LDA) based on the LDA and LDA+*U* exchange-correlation functionals.

2. Crystal structure of Ag_8GeS_6

Synthetic argyrodite melts congruently (with open peak) at 1221 K [3] and 1223 K [2] and undergoes a polymorphic transformation at 488 K [9], 500 K [2]. The low-temperature modification of Ag_8GeS_6 crystallizes in the orthorhombic lattice. Its unit cell contains four Ge atoms, thirty two Ag atoms and twenty four S atoms. The symmetry corresponds to $Pna2_1$ space group. The experimental unit cell parameters are: $a = 15.149 \text{ \AA}$, $b = 7.476 \text{ \AA}$, $c = 10.589 \text{ \AA}$, $Z = 4$ [10]. Our calculated equilibrium parameters are slightly larger: $a = 15.339 \text{ \AA}$, $b = 7.582 \text{ \AA}$, $c = 10.798 \text{ \AA}$.

Ag atoms have three types of coordination in Ag_8GeS_6 crystal structure: distorted tetrahedral (Ag–S 2.56–2.94 Å), flat triangular (Ag–S 2.49–2.76 Å) and linear (S–Ag–S). Germanium atoms are located at the centers of isolated $[\text{GeS}_4]$ tetrahedra (Ge–S 2.200–2.227 Å). All sulfur atoms in Ag_8GeS_6 structure are bridged. Therefore, a complex three-dimensional structure carcass is formed by vertex-linked $[\text{GeS}_4]$, $[\text{AgS}_4]$ tetrahedra and $[\text{AgS}_3]$ triangles. Ag atoms with linear coordination are additionally introduced into the voids of this carcass, thereby it is realized the short contacts Ag–Ag (2.93–3.11 Å) in the structure similar in magnitude to the interatomic distances typical for elementary Ag (2.889 Å).

3. Calculation method

The energy band structure calculations were carried out in the framework of density functional theory [11, 12] using the local density approximation (LDA) as the exchange-correlation potential. As known, the calculations with the LDA approximation give the underestimated band gap values. The electronic spectrum can be described more correctly with account of the Coulomb interaction, which can be achieved in the methods based on density functional theory, but taking into account the interatomic Coulomb and exchange interactions in the framework of the so-called LDA+ U approximation [13]. The magnitude of the Coulomb parameter U was calculated using the linear response described in [14]. The calculations were performed using the SIESTA software package [15, 16].

Total and partial densities of electronic states were determined using the modified tetrahedra method, for which the energy spectrum and the wave functions were calculated on the k -grid containing 15 points. The integration over the irreducible part of Brillouin zone was carried out using the method of special k -points [17, 18]. The total valence charge density $\rho(\mathbf{r})$ was calculated using the integration circuit at special points [18].

4. Electronic structure of Ag_8GeS_6

The electronic structure calculation of Ag_8GeS_6 crystal was performed in the high symmetry points and directions of Brillouin zone (BZ) for the orthorhombic

cell shown in Fig. 2. The energy band structure, total and partial densities of states of Ag_8GeS_6 crystal calculated in the LDA+ U approximation without considering the spin-orbital interaction are shown in Figs. 3 and 4, respectively. The top of valence band is accepted as the energy zero. The calculations in the LDA approximation qualitatively repeat the calculation results in the LDA+ U approximation. According to our calculations, the argyrodite is a direct-gap semiconductor with the dispersion law extremes at the center of Brillouin zone with the band gap width $E_{gd} = 1.46 \text{ eV}$ calculated in the LDA+ U approximation.

The energy spectrum of valence electrons directly determines such an important characteristic of the crystal as the spectral dependence of absorption coefficient. There are two papers [7, 8] devoted to the experimental study of fundamental absorption edge of Ag_8GeS_6 crystals grown by the Bridgman method. It follows from the analysis of fundamental absorption edge that argyrodite really is direct-gap semiconductor with the band gap width $E_{gd}^{opt} = 1.48 \pm 0.05 \text{ eV}$ [6] and $E_{gd}^{opt} = 1.41 \text{ eV}$ [7]. The band gap estimated from the red border of photoconductivity is $E_g = 1.39 \text{ eV}$ [8]. Thus, the account of Hubbard correction in the LDA-Hamiltonian allowed to obtain the band gap value close to the experimental one. Calculation of the argyrodite electronic structure in the LDA approximation gives the value of direct band gap width (direct transition $\Gamma_v \rightarrow \Gamma_c$) $E_{gd} = 0.44 \text{ eV}$, *i.e.* it is significantly underestimated in comparison with the experimental values.

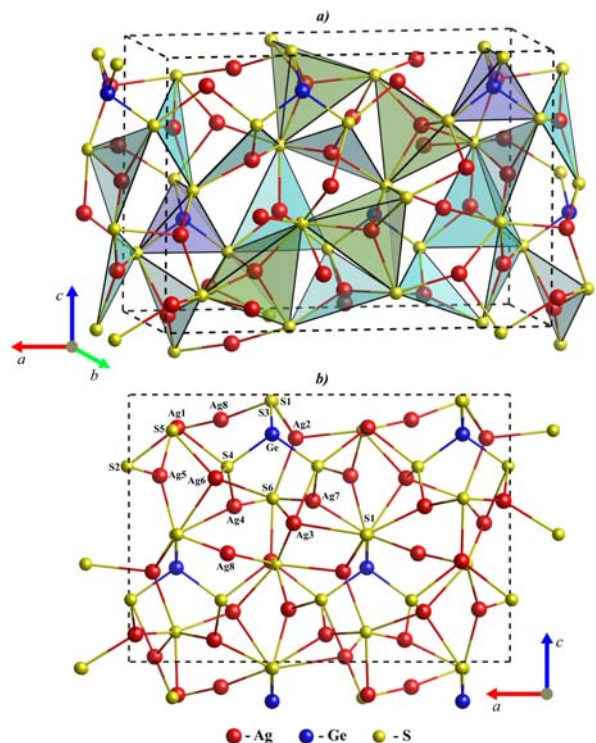


Fig. 1. Crystal structure (a) and the structure projection onto [010] plane (b) of Ag_8GeS_6 .

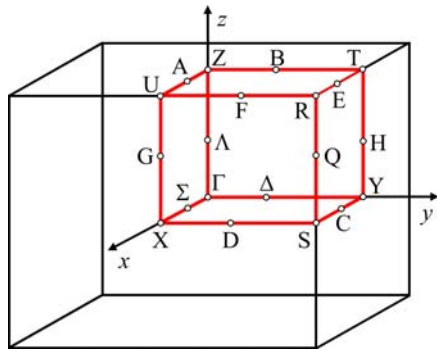


Fig. 2. Brillouin zone of orthorhombic Ag_8GeS_6 .

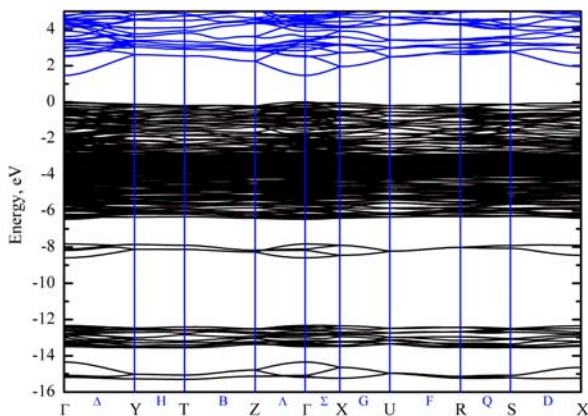


Fig. 3. Electronic structure of Ag_8GeS_6 calculated in the LDA+ U approximation.

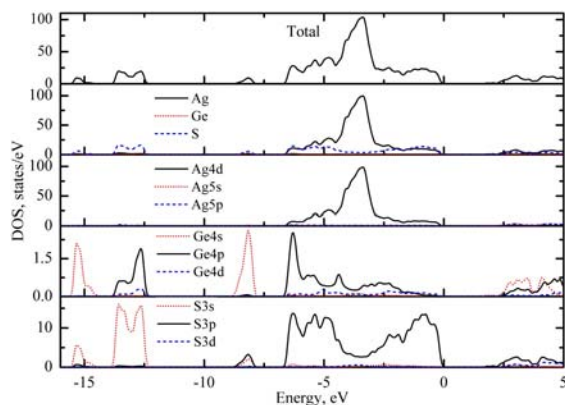


Fig. 4. Total and local partial densities of states in Ag_8GeS_6 calculated using LDA+ U approximation.

The valence band energy spectrum $E(k)$ consists of 256 dispersion branches forming four energy separated valence subbands with a total width 15.3 eV (from the lower edge of $\text{S}3s$ -band to the valence band top). The analysis of partial contributions to the total density of electronic states $N(E)$ (Fig. 4) allows one to identify the genetic nature of the various subbands of occupied states.

From the ion transport viewpoint, the greatest interest is attracted by the formation nature of upper subband of occupied states consisted of 228 dispersion branches and located inside the energy range from 6.47 to 0 eV. This section of the density of electronic states $N(E)$ spectrum (Fig. 4) is formed by $\text{S}3s$ - and $\text{Ag}4d$ -atomic orbitals with a small impurity of $\text{Ge}4p$ -states. The special feature of this electron spectrum section is the splitting of sulfur $3p$ -band into two components and the repulsion of the last ones on both sides of the position of silver $4d$ -band with a strongly marked peak at -3.24 eV. Consequently, the upper valence subband can be separated into three parts. The lower part inside the energy range from -6.47 to -4.44 eV is formed by hybridized $\text{Ag}4d$ - $\text{S}3p$ -states with an insignificant impurity of germanium $4p$ -states. Silver $4d$ -states make the dominant contribution into the middle part (from -4.44 to -2.72 eV) of this subband. The electronic states in the vicinity of the valence band top have mixed anion-cation nature with roughly equal contributions of $\text{Ag}4d$ - and $\text{S}3p$ -states.

The lowest bunch (from -15.3 to -14.35 eV) of four dispersion branches is formed mostly by sulfur $3s$ -states with admixing the germanium $4s$ -states. Next subband (from -13.31 to -12.32 eV) of 20 dispersion branches has very low dispersion, and it is also formed mainly by sulfur $3s$ -states, but with an insignificant impurity of germanium $4p$ -states. These two quasi $\text{S}3s$ -subbands are separated by a gap 3.73 eV from the second subband (-8.6 ÷ -7.84 eV) consisted of four dispersion branches and formed by hybridized sulfur $3s$ -, $3p$ -states and germanium $4s$ -states. Thus, the analysis of total and partial densities of $\text{S}3s$ -, $3p$ - and $\text{Ge}4s$ -, $4p$ -states indicates the significant impurity of germanium and sulfur s -, p -states to each other, which is indicative of the strong covalent nature of chemical bond between Ge and S atoms in the coordination $[\text{GeS}_4]$ tetrahedron that is one of the structural unit in Ag_8GeS_6 .

The lower edge of conduction band has a significant dispersion. The electronic low-energy structure of unoccupied electron states of argyrodite is mainly formed by mixing the empty p -states of sulfur and s , p -states of germanium and silver.

The comparison of the calculated total densities of states $N(E)$ with the experimental X-ray photoelectron spectra (XPS) of GeS_2 , Ag_2S and Ag_8GeS_6 (Fig. 5) allows to observe the changes of electronic structure, which occur with the silver introduction into germanium disulfide at alloying it with Ag_2S and formation of the ternary Ag_8GeS_6 compound. The introduction of silver atoms into GeS_2 leads to increasing the total valence band width, to splitting the bottom $\text{S}3s$ -like subband on two subbands as well as to changing topology of the upper valence subband. Fig. 5 shows that the location, width and intensity of the major structural features in the XPS spectra related with silver $4d$ -states are close to the calculated values in $N(E)$ spectra of Ag_2S and Ag_8GeS_6 . Thus, the theoretical calculation gives the well observed

admiring the sulfur $3p$ -states to silver $4d$ -states, which is understandable in the formation of Ag–S chemical bonds in Ag_8GeS_6 .

5. The effective masses of electrons and holes

The effective masses of charge carriers depend on the same matrix elements of the momentum operator between energy bands that determine the value of the optical absorption due to the direct transitions. In this case, it was taken into account that the tensor components of reciprocal effective masses are determined by the second-order derivatives from the energy of one-electron states on the wave vector Cartesian coordinates $\mathbf{k} = (k_x, k_y, k_z)$ at the extremum point:

$$\frac{1}{m_{\alpha\beta}} = \frac{1}{\hbar^2} \frac{\partial^2 E(k_0)}{\partial k_\alpha \partial k_\beta}. \quad (1)$$

The effective masses of electrons (m_e^*) and holes (m_h^*) in argyrodite crystal were received by the quadratic approximation of calculated dispersion law $E(\mathbf{k})$ at the extrema vicinity in the center of Brillouin zone using the Eq. (1). Table shows the values of effective masses of electrons and holes with the corresponding directions in the reciprocal space calculated in the LDA and LDA+ U approximations. The table shows that the effective masses of electrons and holes obtained in the LDA+ U calculations become larger. By now, the experimentally effective masses of electrons and holes in crystalline Ag_8GeS_6 are not determined.

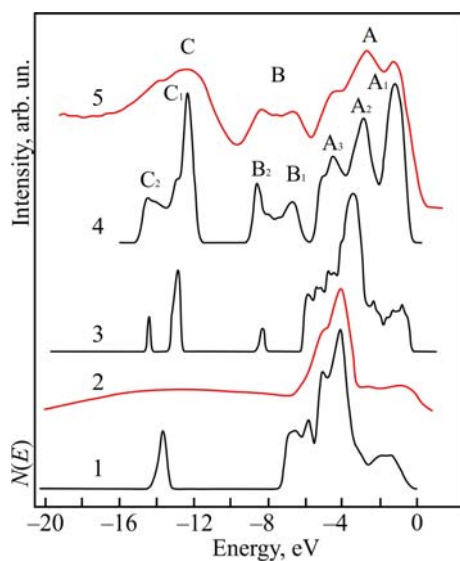


Fig. 5. Comparison of the smoothed calculated total densities of states (1, 3, 4) in the valence band of crystalline Ag_2S (1), Ag_8GeS_6 (3) and GeS_2 (4) with the experimental XPS spectra of crystalline Ag_2S (2) [19] and GeS_2 (5) [20].

Table. The values of effective masses of electrons m_e^* and holes m_h^* in Ag_8GeS_6 . They are given in units m_0 .

Calculation type	Direction	$\Gamma \rightarrow X$	$\Gamma \rightarrow Z$	$\Gamma \rightarrow Y$
LDA	m_e^*/m_0	0.12	0.15	0.17
	m_h^*/m_0	-0.26	-1.07	-1.07
LDA+ U	m_e^*/m_0	0.24	0.28	0.29
	m_h^*/m_0	-0.41	-1.49	-1.42

6. Spatial distribution of valence charge density

Formation of main interparticle interactions in the orthorhombic Ag_8GeS_6 phase can be clearly observed using the distribution of total charge density $\rho(\mathbf{r})$. The complex crystal structure of argyrodite complicates representation of contour maps in the available 2D format. In this case, it is the most convenient to present the electronic configurations in the planes that pass through two sulfur atoms and one Ge(Ag) atom in $[\text{GeS}_4]$, $[\text{AgS}_4]$ tetrahedra and $[\text{AgS}_3]$ triangle (Figs. 6a–6c), along linear coordination S–Ag–S (Fig. 7), along plane passing through two $[\text{AgS}_3]$ triangles linked together by the $[\text{GeS}_4]$ tetrahedron (Fig. 8) and along plane passing through linked to each other the $[\text{GeS}_4]$ tetrahedron, $[\text{AgS}_3]$ triangle and S–Ag–S (Fig. 9).

The contour maps clear show that the charge density is concentrated mainly in the indicated structural units and the silver atom contributions occupy more noticeable part of the space than sulfur atom contributions and even more than germanium atoms.

The valence electron charge in $[\text{GeS}_4]$ tetrahedra is distributed primarily on the sulfur atom with strong contour deformations in the direction to germanium atoms. It can also be seen from the maps that there are the localized maximums on the Ge–S bonds in $[\text{GeS}_4]$ tetrahedra, and they are combined by the common contours. The strongly pronounced deformation of contours $\rho(\mathbf{r})$ in the direction from the sulfur atoms to the germanium ones along Ge–S bond line and the presence of the overall contours covering the electron density maximums in the cation-anion bonds (Fig. 6a) reflect the covalent component of the chemical bond in $[\text{GeS}_4]$ tetrahedra caused by hybridization of $\text{Ge}4s$ -, $4p$ - and $\text{S}3p$ -states (Fig. 4). The ionic chemical bond component in $[\text{GeS}_4]$ tetrahedra is caused by the partial transfer of charge density from germanium atoms to more electronegative sulfur atoms. It is reflected on the electron density maps by a higher density of valence electrons near the localization places of sulfur atoms.

The main charge in the structural units formed with participation of Ag atoms is concentrated on the silver atoms, and it has the form of closed and almost spherical

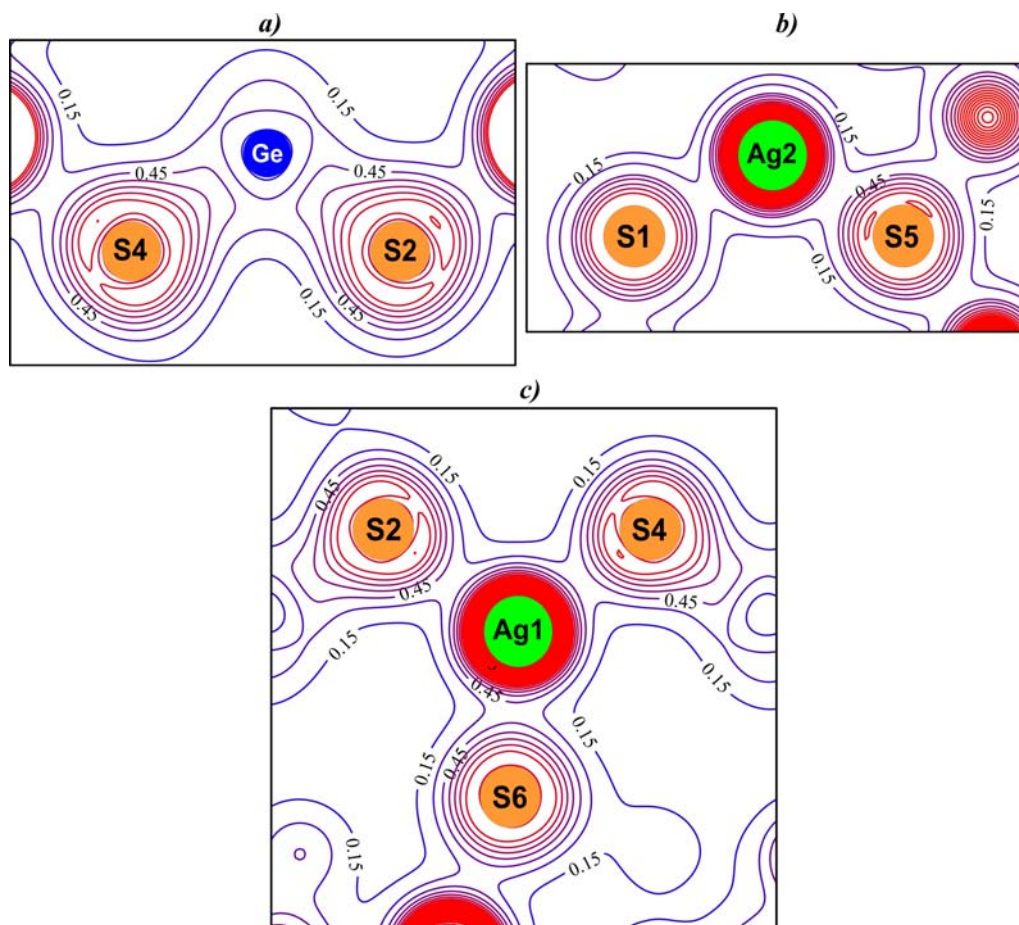


Fig. 6. Electronic density maps in the planes passing along Ge-S bond line in [GeS₄] tetrahedron (a), along Ag-S in [AgS₄] tetrahedron (b) and [AgS₃] triangle (c).

contours with very small polarization (Figs. 6b and 6c). The charge transfer from the noble metal atoms to sulfur atoms leads to electrostatic interactions and creates an ionic component of the interatomic bond. In addition, there are several types of bonding and antibonding covalent interactions. The most important of those are bonds of silver *d*-electrons and sulfur *p*-electrons. Overall contours covering cation Ag and anion S atoms precisely characterize the covalent component of chemical bond in this compound, which although is small but nevertheless occurs.

Furthermore, Figs. 8 and 9 clearly show that the valence electron density has the overall contours for various structural units linked to each other through the bridged sulfur atoms. However, the deformation nature of contours on anion-cation bond lines around common sulfur atoms connecting neighbor [GeS₄], [AgS₄] tetrahedra and [AgS₃] triangles differs significantly. Thus, the contours around a chalcogen are stronger deformed in the direction to germanium atom along S-Ge bond line, than along S-Ag bond line (Figs. 8, 9).

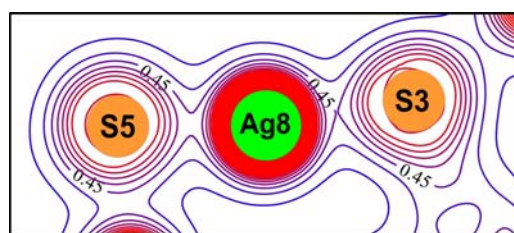


Fig. 7. Electronic density distribution map in the plane passing along the linear coordination S-Ag-S.

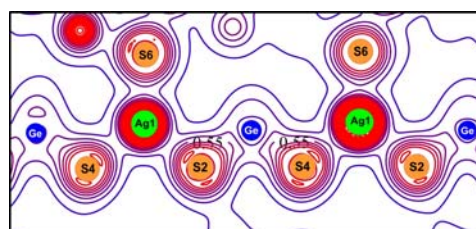


Fig. 8. Electronic density distribution map in the plane passing parallel to the *b*-axis of Ag₈GeS₆ crystal.

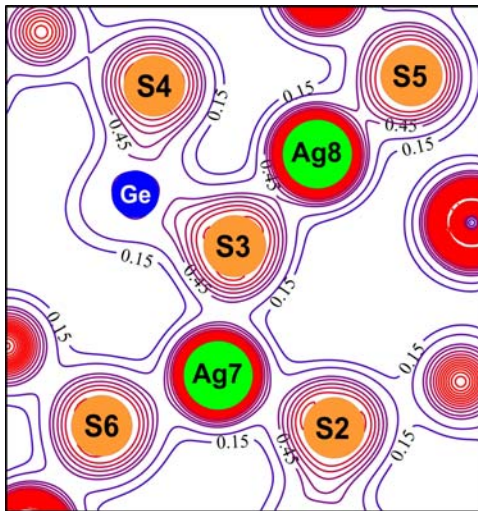


Fig. 9. Electronic density map along the plane passing through linked together $[\text{GeS}_4]$ tetrahedron, $[\text{AgS}_3]$ triangle and S–Ag–S bond line.

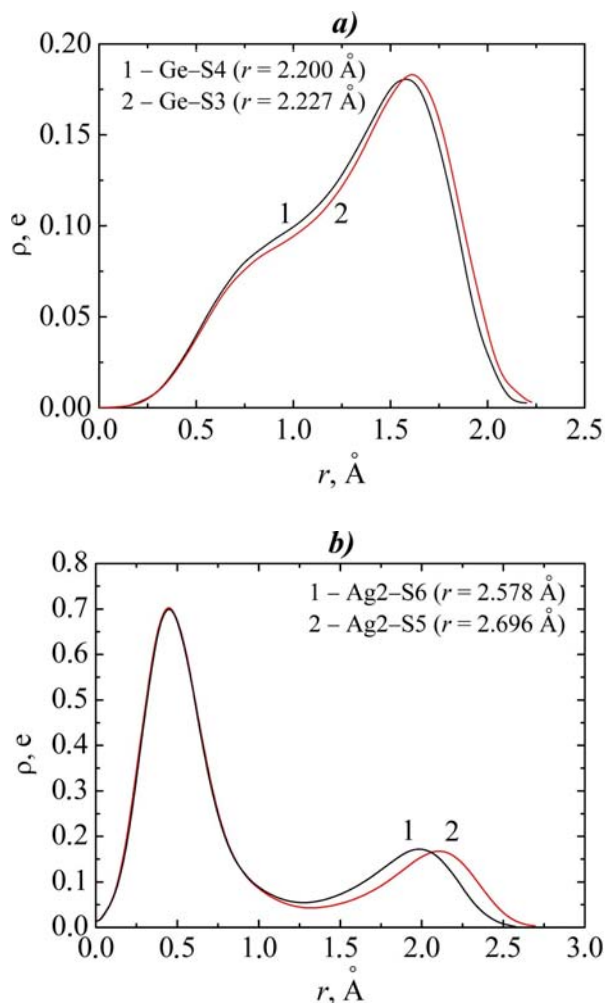


Fig. 10. The radial charge density distribution in $[\text{GeS}_4]$ (a) and $[\text{AgS}_4]$ (b) tetrahedra.

Thus, the nature of total electron density contours $\rho(\mathbf{r})$ in Ag_8GeS_6 crystal shows the ion-covalent type of bonding. The difference of chemical nature of Ag and Ge atoms determines the difference of Ag–S and Ge–S chemical bonds. The Ag–S bond is more ionic than the Ge–S one, at the same time, the Ag–S bond is weaker than the Ge–S one.

The character of formed interatomic bonds in the specific structural units of Ag_8GeS_6 crystal can be also illustrated using the spatial distribution of the radial charge densities ($4\pi nr^2$). Fig. 10 presents the $4\pi nr^2$ values of atoms in $[\text{GeS}_4]$ and $[\text{AgS}_4]$ tetrahedra. It is seen that the anion charge density in $[\text{GeS}_4]$ tetrahedron has a pronounced local maximum near the nucleus, whereas it is less pronounced near the cation (Ge). Conversely, the charge density in $[\text{AgS}_4]$ tetrahedron is minimal near the anion, and it is mainly concentrated in the vicinity of silver atoms.

It is also possible to estimate the type of chemical bonds in the crystal by using the atomic charge values and the valence electronic density redistribution. The atomic charges of Ag_8GeS_6 crystal calculated using the Mulliken model have the following values (in e units): 10.580–10.704 for Ag atoms, 3.922 for Ge atoms, 6.368–6.694 for S atoms; and they well correlate with the atomic electronegative values: 2.58 for S, 2.01 for Ge, 1.93 for Ag. It is well known that the bond polarity is greater when the electronegativity difference of bonding atoms is larger. If the difference is higher than two units, then the ionic component is almost always predominant. It is known that the lower charge, the higher polarizability of electron shell, and the radius close to 1 Å of silver-cation allows to designate it to the category of the so-called “magic ions”, which are typical for the compounds with high ionic conductivity [21].

7. Conclusions

For the first time, the energy band structure, total and partial densities of states for Ag_8GeS_6 crystal were calculated using the *ab initio* density functional method in the LDA and LDA+ U approximations. According to the calculation results, the argyrodite is a direct-gap semiconductor with the localization of valence band top and the conduction band bottom at the Γ point of Brillouin zone. The band gap width E_{gd} is 1.46 eV in the LDA+ U approximation, which agrees well with the experimental values obtained from the analysis of fundamental absorption edge of Ag_8GeS_6 crystal.

The electronic density $\rho(\mathbf{r})$ was calculated, and the spatial distribution maps of valence electronic charge in the plane passing along Ge(Ag)–S bond lines in the different structural units of Ag_8GeS_6 crystal structure were plotted, which allowed to describe the formation features of chemical bonds between atoms forming this crystal. The effective mass values for electrons and holes in Ag_8GeS_6 were estimated.

References

1. Moh G.H. Experimental and descriptive ore mineralogy. *Neues Jahrbuch für Mineralogie – Abhandlungen*. 1976. **128**, No. 2. P. 146–152.
2. Kokhan A.P. The interaction in $\text{Ag}_2\text{X}-\text{B}^{\text{IV}}\text{X}_2$ ($\text{B}^{\text{IV}} - \text{Si, Ge, Sn; X = S, Se}$) systems and properties of compounds: Abstract of Dissertation ... Cand. Sci. (Chem.), Uzhhorod, 1996. 21 p.
3. Olekseyuk I.D., Kogut Y.M., Fedorchuk A.O., Piskach L.V., Gorgut G.P., Parasyuk O.V. The $\text{Ag}_2\text{S}-\text{GeS}_2$ system and Ag_2GeS_3 crystal structure. *Naukovyi visnyk Volyns'koho Natsional'noho Universytetu im. Lesi Ukrainky. Neorhanichna Khimii*. 2010. **16**. P. 25–33 (in Ukrainian).
4. Petrov A.V., Orlov V.M., Zaitsev V.K., Feigel'man V.A. Characteristic of the thermal conductivity of Ag_8MX_6 compounds having complex crystal structures. *Fiz. Tverd. Tela*. 1975. **17**. P. 3703–3705 (in Russian).
5. He Q., Qian T., Zai J., Qiao Q., Huang S., Li Y., Wang M. Efficient Ag_8GeS_6 counter electrode prepared from nanocrystal ink for dye-sensitized solar cells. *J. Mater. Chem. A*. 2015. **3**, No. 40. P. 20359–20365.
6. Osipishin I.S., Gasii B.I., Butsko N.I. The investigation of fundamental absorption edge of argyrodite and canfieldite crystals. *Fiz. Tekh. Poluprovodn.* 1974. **10**, No. 8. P. 1609–1611 (in Russian).
7. Kinduris A.S., Bendorius R.A., Senulene D.B. The changes of fundamental absorption edge of $\text{Ag}_8\text{M}^{\text{IV}}\text{X}^{\text{VI}}_6$ at the polymorphic transformations. *Fiz. Tekh. Poluprovodn.* 1976. **10**, No. 8. P. 1544–1547 (in Russian).
8. Osipishin I.S., Butsko N.I., Gasii B.I., Zhezhnich I.D. Thermally stimulated conductivity and photoelectric properties of argyrodite and canfieldite. *Fiz. Tekh. Poluprovodn.* 1972. **6**, No. 6. P. 1121–1123 (in Russian).
9. Chbani N., Cai X., Loireau-Lozac'h A.M., Guittard M. Ternaire argent-germanium-sulfure. Quasibinaire disulfure de germanium – sulfure d'argent. Conductivite electrique du verre le plus riche en argent. *Mater. Res. Bull.* 1992. **27**, No. 11. P. 1355–1361.
10. Eulenberg G. Die Kristallstruktur der Tieftemperaturmodifikation von Ag_8GeS_6 – Synthetischer Argyrodit. *Monatshefte für Chemie*. 1977. **108**. P. 901–913.
11. Hohenberg P., Kohn W. Inhomogeneous electron gas. *Phys. Rev.* 1964. **136**, No. 3. P. B864–B871.
12. Kohn W., Sham L.J. Self-consistent equations including exchange and correlation effects. *Phys. Rev.* 1965. **40**, No. 4. P. A1133–A1138.
13. Anisimov V.I., Aryasetiawan F., Lichtenstein A.I. First-principles calculations of the electronic structure and spectra of strongly correlated systems: the LDA+U method. *J. Phys.: Condens. Matter*. 1997. **9**, No. 4. P. 767–808.
14. Cococcioni M., de Gironcoli S. Linear response approach to the calculation of the effective interaction parameters in the LDA+U method. *Phys. Rev. B*. 2005. **71**. P. 035105-1–035105-16.
15. Soler J.M., Artacho E., Gale J.D., Garcia A., Junquera J., Ordejón P., Sánchez-Portal D. The SIESTA method for ab initio order-N materials simulation. *J. Phys.: Condens. Matter*. 2002. **14**, No. 11. P. 2745–2779.
16. <http://icmab.cat/leem/siesta/>
17. Chadi D.J., Cohen M.L. Special points in the Brillouin zone. *Phys. Rev. B*. 1973. **8**, No. 12. P. 5747–5753.
18. Monkhorst H.J., Pack J.D. Special points for Brillouin-zone integrations. *Phys. Rev. B*. 1976. **13**, No. 12. P. 5188–5192.
19. Kashida S., Watanabe N., Hasegawa T., Iida H., Mori M., Savrasov S. Electronic structure of Ag_2S , band calculation and photoelectron spectroscopy. *Solid State Ionics*. 2003. **158**, No. 1-2. P. 167–175.
20. Foix D., Gonbeau D., Granier D., Pradel A., Ribes M. Electronic structure of thiogermanate and thioarsenate glasses: experimental (XPS) and theoretical (ab initio) characterizations. *Solid State Ionics*. 2002. **154-155**. P. 161–173.
21. Il'ina A.A., Stenina I.A., Lysanova G.V., Yaroslavtsev A.B. Synthesis and ionic conductivity of silver magnesium zirconium molybdates. *Inorganic materials*. 2009. **45**(4), P. 436–439.